J Mol Model (2011) 17:3005–3013
DOI 10.1007/s00894-011-0985-8

ORIGINAL PAPER

The influence of tether number and location on the self-assembly of polymer-tethered nanorods

Li Zhao · Xiang-Gui Xue · Zhong-Yuan Lu · Ze-Sheng Li

Received: 17 November 2010 / Accepted: 24 January 2011 / Published online: 1 March 2011

Abstract Coarse-grained molecular dynamics simulations were used to investigate the self-assembly of polymer-tethered nanorods with relatively high aspect ratio. The number and location of polymer tethers were varied to determine their influence on nanorod self-assembly. We found that laterally polymer-tethered nanorods self-assemble into structures with flat interfaces; these structures include stepped ribbons, stepped lamellae and lamellae with rods packed into bilayer sheets. The stepped lamellar phase is observed for the first time in this study. End polymer-tethered nanorods are prone to self-assemble into structures with curved interfaces, and the assembled structures observed here include spherical micelles and nematically aligned cylinders. The cylinder phase exists at high number densities, instead of the lamellar phase typically found for end polymer-tethered nanorods with relatively lower aspect ratio.

Keywords Self-assembly · Polymer-tethered nanorod · Molecular dynamics simulation

Electronic supplementary material The online version of this article (doi:10.1007/s00894-011-0985-8) contains supplementary material, which is available to authorized users.

L. Zhao · X.-G. Xue · Z.-Y. Lu (✉) · Z.-S. Li (✉)
Institute of Theoretical Chemistry, State Key Laboratory of Theoretical and Computational Chemistry, Jilin University, Changchun 130023, China
e-mail: luzhy@jlu.edu.cn

Z.-S. Li
e-mail: zeshengli@jlu.edu.cn

Z.-S. Li
Department of Chemistry, School of Science, Beijing Institute of Technology, Beijing 100081, China

Introduction

Polymer-tethered nanoparticles have attracted increasing interest in recent years as promising building blocks that self-assemble into highly ordered nanostructures. Self-assembled structures on the nanoscale have important implications for the fabrication of novel electronic and photonic materials [1–4]. Moreover, the local packing of rigid nanoparticles gives rise to additional orientational ordering within the self-assembled nanostructures. A wide variety of complex structures, such as micelles, wires, and sheets, has been reported. The emergence of these structures has been explained by competition between the entropy contributed by the polymer tethers and the maximization of nanoparticle–nanoparticle contacts [5].

Computer simulations have been applied successfully to predict the self-assembled structures of polymer-tethered nanoparticles and investigate the factors influencing the self-assembly process and structure. The self-assembly behavior of polymer-tethered nanoparticles with different shapes, including rodlike [6–18], spherical [6, 19, 20], cubic [21–24], V-shaped [25], disklike [26, 27], and other shaped nanoparticles [5] has been investigated extensively, and the results suggested that anisotropic interactions significantly affect the self-assembled morphologies. The anisotropicity of the interactions is induced mainly by the location, length, and number of polymer tethers, as well as by the shape of nanoparticles (shape effect). Glotzer and co-workers have studied the self-assembly behavior of polymer-tethered nanorods systematically [6–10], and have predicted a wide variety of self-assembled morphologies, including spherical micelles, long micelles, hexagonally ordered cylinders, perforated phases and lamellar phases, when polymers were tethered on the end bead of the

nanorod [7–9], and stepped-ribbon-like micelles, centered rectangular stepped-ribbon phase, and liquid crystalline bilayer phases when polymers were tethered on the middle bead of the nanorod [10]. These authors also presented and compared the inverse temperature versus relative tether fraction phase diagrams for end polymer-tethered nanorods with low and moderate aspect ratios. In addition, end-tethered nanorods with low, moderate and high aspect ratios were observed to form different morphologies for similar coil fraction. For example, high aspect ratio rods self-assemble into zigzag lamellar morphologies, while moderate and low aspect ratio rods form smectic C morphologies. However, only long rods with small tether fractions were investigated because of the limitation of high computational labor. Crane et al. [11] reported on the self-assembly behavior of a rodlike bolaamphiphilic model with a lateral flexible chain of different lengths. The molecules self-assemble into smectic, columnar and lamellar phases as the length of polymer tethers increases. Bates and Walker [12] examined the influence of the number and length of polymer tethers connecting the central aromatic rod-like core; they predicted square, hexagonal columnar and lamellar phases as the polymer tether length is increased. In their study, the columnar structure is double-walled for molecules with one polymer tether and single-walled for molecules with two polymer tethers.

Although the influence of the number and location of polymer tethers on the self-assembly of polymer-tethered nanorods was referred to in the above-mentioned research, a comparative study on the detailed influence of these factors is still lacking. Therefore, in this study, we apply a coarse-grained molecular dynamics (CGMD) simulation to study the self-assembly behavior of polymer-tethered nanorods with different numbers and different locations of polymer tethers. As a useful simulation technique, CGMD has been applied successfully to the study of the self-assembly behavior of nanoparticles [11, 28, 29]. Here, we present the temperature versus number density phase diagrams for the systems of laterally tethered and end-tethered nanorods with relatively high aspect ratio. The paper is organized as follows: Model and simulation methods exhibits the simulation model and the computational details, the Results and discussion section presents the simulation results and the corresponding discussion, followed by a final Conclusion.

Model and simulation methods

The nanorod consists of nine coarse-grained (CG) beads linked rigidly in a linear geometry. We considered only the symmetric composition of the system, i.e., the number of tethered CG beads is also nine. Both the inter-bead distance and the diameter of a bead are σ—the characteristic length of the model in our study. The flexible tethers are modeled as linear, bead-spring chains. The beads in the tethers are bonded together via a harmonic potential of the form

$$U_{harm} = \frac{1}{2} k_{sp} (r - r_0)^2 \quad (1)$$

where k_{sp} is the spring constant, r is the distance between neighboring beads, and r_0 the equilibrium separation. The values of k_{sp} and r_0 are taken as $50(\varepsilon/\sigma^2)$ and σ, respectively, in which ε is the characteristic energy of the model in our study [11]. Bonded interactions between the flexible tethers and the rods are also described by the harmonic potential with the same parameters as shown above. It is worth noting that, in such a CG model, each bead represents a group of atoms, and that simulations could capture the mesoscopic behavior of tethered nanorods, as illustrated by other studies [6–11].

Five types of tethered nanorods are considered in our study, and their topologies are shown in Fig. 1. The first three models are laterally tethered nanorods denoted by TN1-5, TN1-3, and TN3-258, respectively. The number before "-" means the number of tethers on the nanorod, and the number after "-" means the tether position along the nanorod, for example, TN1-5 means one nine-bead tether attached to the middle of the nanorod, TN1-3 means one nine-bead tether attached to the third bead of the nanorod, and TN3-258 means three three-bead tethers attached to the second, fifth, and eighth bead of the

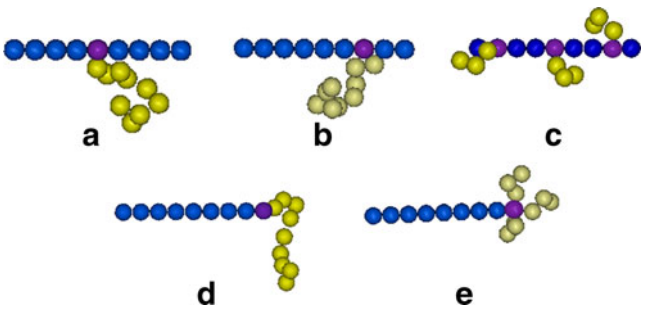

Fig. 1 **a**–**e** Tethered nanorod models. **a** TN1-5, laterally tethered nanorod with one nine-bead tether grafted on the middle bead; **b** TN1-3, laterally tethered nanorod with one nine-bead tether grafted on the third bead, **c** TN3-258; laterally tethered nanorod with three three-bead tethers grafted on the second, fifth and eighth bead; **d** TN1-1, end-tethered nanorod with one nine-bead tether grafted on the end bead; **e** TN3-1, end-tethered nanorod with three three-bead tethers grafted on the end bead. Nanorod beads grafted with tethers are colored *purple*

nanorod. The other two models are end-tethered nanorods denoted by TN1-1 and TN3-1, respectively, which possess one nine-bead tether and three three-bead tethers attached to the end bead of the nanorod, respectively.

In order to study nanorod self-assembly behavior, non-bonded interactions between nanorods are defined to attract each other through an inter-CG bead Lennard-Jones (LJ) potential,

$$U_{LJ}(r) = 4\varepsilon\left[\left(\frac{\sigma}{r}\right)^{12} - \left(\frac{\sigma}{r}\right)^{6}\right] \quad (2)$$

which is truncated at r_{cutoff}=2.5. Non-bonded interactions between tethers, as well as between tethers and rods, are treated using a purely repulsive inter-CG bead Weeks-Chandler-Andersen (WCA) potential,

$$U_{WCA}(r) = 4\varepsilon\left[\left(\frac{\sigma}{r}\right)^{12} - \left(\frac{\sigma}{r}\right)^{6}\right] + \varepsilon \quad (3)$$

The WCA potential is the LJ potential truncated at the minimum and shifted vertically by the well depth. In our simulations, the mass of each bead is set as m for simplicity. The reduced temperature, $T^*=k_BT/\varepsilon$, where k_B is Boltzmann constant, the reduced pressure, $P^*=P\sigma^3/\varepsilon$, and the time unit is $\tau = \sigma\sqrt{m/\varepsilon}$.

Molecular dynamics simulations were performed using the simulation suite DL_POLY version 2.18 [30]. Integrations are carried out using the velocity Verlet algorithm and NOSQUISH [31] for the rigid part, with a time step of $\Delta t = 2\times10^{-4}\tau$. Temperature control is achieved by means of Berendsen thermostat and pressure is controlled by Berendsen barostat.

Systems with N=500 nanorods, corresponding to a total number of beads of N_b=9,000, were studied. The bead number density φ ranges from 0.1 to 0.7. The systems are treated initially only with repulsive WCA potential at high temperature to obtain isotropic phases. Simulations are then performed in the canonical ensemble where total number of beads, volume and temperature are fixed. The systems are quenched following a stepping schedule with a temperature step ΔT^*=0.1. At each intermediate temperature, the simulations are performed at least 10^8 time steps until the potential energy fluctuates about a constant value. To ascertain that any observed phases are not affected by finite size effect, a series of simulations are performed in the isotension-isothermal ensemble, where total number of beads, the components of the stress tensor, and temperature, are fixed. In the isotension–isothermal ensemble, both the size and shape of the simulation box are allowed to change during the simulation, thus the isotension–isothermal ensemble can ensure equality of pressure in all three directions.

Results and discussion

Laterally tethered nanorods

Laterally tethered nanorods form both stepped ribbon phase and lamellar phase. The morphological phase diagrams of these tethered nanorods are presented in Fig. 2. We find that rod–rod interactions dominate the self-assembly process, and that equilibrium structures with flat interfaces are preferred. Specifically, for TN1-5 and TN1-3, we observed a stepped ribbon phase and a new stepped lamellar phase,

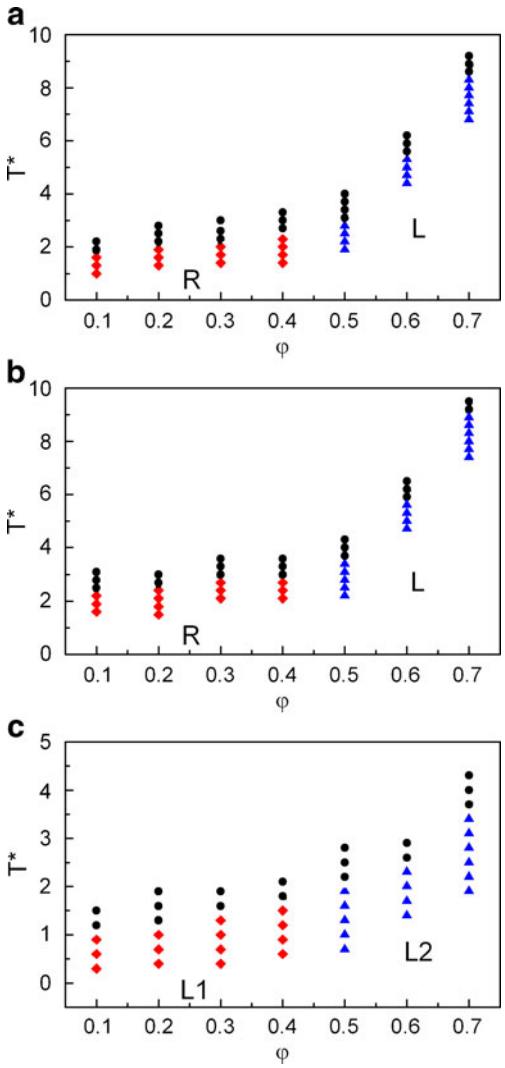

Fig. 2 **a**–**c** Temperature vs number density phase diagrams. **a** Phase diagram for TN1-5. *Red diamonds* Stepped ribbon phase (*R*), *blue triangles* stepped lamellar phase (*L*). **b** Phase diagram for TN1-3. *Red diamonds* Stepped ribbon phase (*R*), *blue triangles* stepped lamellar phase (*L*). **c** Phase diagram for TN3-258. *Red diamonds* Lamellar phase with low ordering (*L1*), *blue triangles* lamellar phase with high ordering (*L2*), *black circles* disordered states

but for TN3-258, we found a lamellar phase with nanorods packed into two-layered sheets. We have also repeated the simulations with different initial configurations to ascertain the obtained phase structures. Further discussion on the typical self-assembly structures is given below.

Self-assembly of laterally tethered nanorod with a nine-bead tether

TN1-5 At low number densities where φ varies from 0.1 to 0.4, an infinite stepped ribbon phase for the nanorod aggregates with rectangular cross section perpendicular to the general direction of the rods is observed at lower temperatures. Figure 3a is a typical snapshot for a system at φ=0.3 and T^*=1.9. To describe the orientational ordering of the nanorods in the self-assembly structures, the orientational order parameter Q is calculated from the following tensor,

$$\Omega_{\alpha\beta} = \frac{1}{N}\sum_{i=1}^{N}\frac{3u_{i\alpha}u_{i\beta} - \delta_{\alpha\beta}}{2} \quad (4)$$

where $u_{i\alpha}(\alpha,\beta$=x, y, z) is the direction cosine of a unit vector describing the direction of the ith nanorod and N is the number of tethered nanorods. The $\Omega_{\alpha\beta}$ tensor is calculated per 5×10^3 time steps, accumulated for 20 consecutive time steps, and then averaged and diagonalized. The orientational order parameter is taken as the largest eigenvalue of the diagonalized $\Omega_{\alpha\beta}$ tensor. The high level of orientational ordering of the system in Fig. 3a is indicated by the orientational order parameter of Q=0.951±0.007. To illustrate the packing of the rods, an individual ribbon extracted from the simulation box is shown in Fig. 3b. Within the ribbons, the rods pack parallel to each other to form a rectangular entity with a constant width of approximately 6.0σ. The offset between steps is about 5.0σ, which is in accordance with the attachment point of the tether on the rod. Unlike laterally tethered nanorods with lower aspect ratio [10], we do not observe phases with finite size micelles at low number densities. This may be due to the fact that the rods with high aspect ratio tend to grow easily along the direction of the rod, and then the infinite stepped ribbon phase appears.

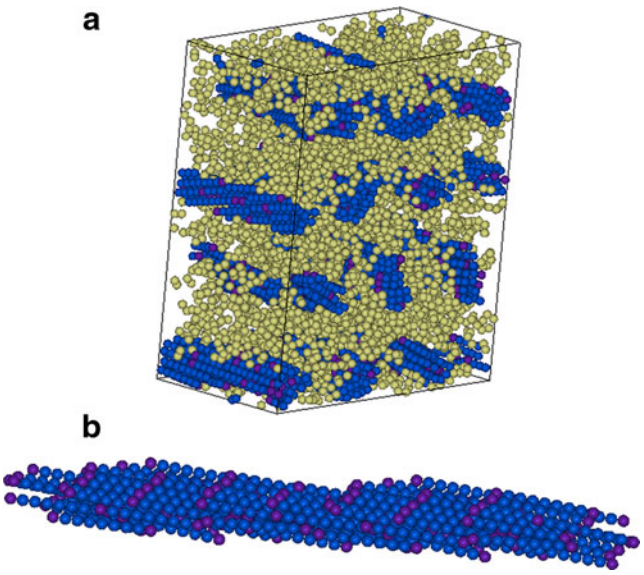

Fig. 3 **a** Stepped ribbons formed by TN1-5 at φ=0.3 and T*=1.9. Rod ends are colored *purple*. **b** A single ribbon structure extracted from the simulation box; the tethers have been removed for clarity

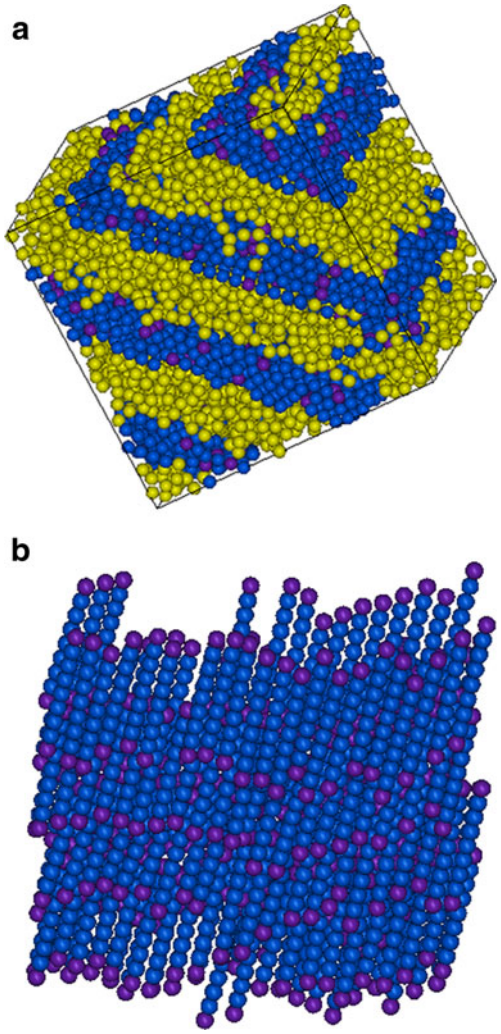

Fig. 4 **a** Stepped lamellae formed by TN1-5 at φ=0.7 and T*=5.0. Rod ends are colored *purple*. **b** A single lamellar structure extracted from the simulation box; the tethers have been removed for clarity

As the number density is increased to φ>0.4, stepped ribbons merge and form stepped lamellar phase even at higher temperatures. As far as we know, such stepped lamellar phase have not been reported previously. A typical snapshot for a system with φ=0.7 and T^*=5.0 is shown in Fig. 4. Moreover, we determine the planar order parameter, which describes the degree to which nanorods

orientation vectors lie in a plane. Firstly, a director is defined by $v_{ij\alpha} = \mu_i \times \mu_j$, where μ_i is the direction cosine of the *i*th nanorod, and $v_{ij\alpha}$(α=x, y, z) is the cross product of the *i*th and *j*th direction cosine of all the nanorod orientation vectors. Then, we can define the tensor

$$\Omega_{\alpha\beta} = \frac{2}{N(N-1)} \sum_{i=1}^{N} \sum_{j>i}^{N} \frac{3v_{ij\alpha}v_{ij\beta} - \delta_{\alpha\beta}}{2} \quad (5)$$

The eigenvector associated with the largest eigenvalue of the diagonalized Ω tensor is defined as the director normal to the plane. Knowing the director orientation, the planar order parameter, S_2, which measures how orthogonal the nanorods orientation vectors are to the director, can be calculated immediately by [11]

$$S_2 = \frac{1}{N} \sum_{i=1}^{N} \left(3\sin^2\theta_i - 2\right) \quad (6)$$

where θ_i is the angle between the director and the orientation vector of the *i*th nanorod. For an isotropically orientated system, the planar order parameter is close to zero, and for ordered system where all the orientation vectors lie in one plane orthogonal to the director, the planar order parameter takes a value close to 1. We find that for the lamellar structures of TN1-5 model, S_2 is always close to 1. For example, for the system with φ=0.7 and T^*=5.0, the value of planar order parameter, S_2=0.947± 0.017 indicates the high level of planar ordering. Within the lamellae, the rods pack and align in the same direction and the offset of the step (5.0σ) is approximately the same as that in low number density cases. In addition, the lamellar phase observed here is quite different from that formed by tethered nanorods with lower aspect ratio [10]. The emergence of the stepped lamellar structure is the result of competition between maximizing rod–rod contacts, and the entropic effect contributed by the tethers. The rod–rod interactions in the system of high aspect ratio nanorods are dominant and stepped lamellae form, whereas bilayer sheets exist for systems composed of lower aspect ratio nanorods [10].

TN1-3 To clarify the influence of tether location on the self-assembly structure of laterally tethered nanorods, we further studied the TN1-3 system, for which the nine-bead tether is grafted onto the third bead of the nanorod. Like TN1-5, the TN1-3 system forms stepped ribbon for φ<0.4 at higher temperatures, and stepped lamellar structures for φ>0.4 at relatively higher temperatures. As shown in the typical snapshot of infinite stepped ribbon phase at φ=0.3 and T^*=1.9 (see electronic supplementary material, Fig. S1), the rods pack parallel to each other but the offset is not constant within the ribbon. However, the orientational ordering is similar to that of TN1-5 system as the orientational order parameter of the system (Fig. S1) is calculated to be Q=0.959± 0.013. As the number density increases, the planar order parameter is again adopted to describe the planar ordering of the lamellar phase at φ=0.7 and T^*=5.8 (Fig. S2), and the calculated value is S_2=0.937±0.086. The offset distribution of rods within the lamellae is similar to that in the ribbon phase. When the nanorod model changes from TN1-5 to TN1-3, the tether location is shifted to the third bead of the nanorod from the middle, therefore the symmetry of the tethered nanorods is broken, and local packing order is slightly decreased.

To quantify the mobility of the laterally tethered nanorods, we calculate the mean squared displacements (MSDs). For ribbon phase formed by TN1-5 and TN1-3 at low number densities, MSDs are resolved into two components: one along the direction of the rods and the other vertical to the direction of the rods. MSDs (Fig. S3) suggest that rods have larger mobility along the direction of the rods for TN1-5, while the two components of the MSDs of rods in TN1-3 system are almost the same. For lamellar phase formed at larger number densities, MSDs are again resolved to two components: one is vertical to the lamellar plane and the other is in the lamellar plane. The component in the lamellar plane of TN1-5 and TN1-3 is apparently dominant.

Self-assembly of laterally tethered nanorod with three three-bead tethers

TN3-258 To investigate the influence of tether number on the self-assembly structures, the phase behavior of laterally tethered nanorods with three three-bead tethers grafted on the second, fifth and eighth bead were examined. Here we observed a lamellar phase in which nanorods pack into bilayer sheets with low and high orientational ordering for number densities below and above 0.4, respectively. Figure 5 shows a typical snapshot for a system with low orientational ordering at φ=0.3 and T^*=1.3. For this system, the calculated planar order parameter S_2=0.974± 0.019 indicates the high level of planar ordering. However, within the sheet, the rods actually orientate randomly. The rods firstly self-assemble into a bilayer block in which the rods pack along the same direction, then the blocks aggregate into infinite bilayer sheets without any common orientation of the nanorods. Figure 6 presents a typical snapshot for a system with high orientational ordering at φ=0.6 and T^*=2.0. The high level of the planar ordering of the system in Fig. 6 is indicated by the value of S_2=0.966±0.031. At high number densities, the rods in a sheet pack end-to-end and parallel to each other. However, the rods crowd tightly and the interfaces are less smooth than those at lower number densities. MSD is again employed to determine the mobility

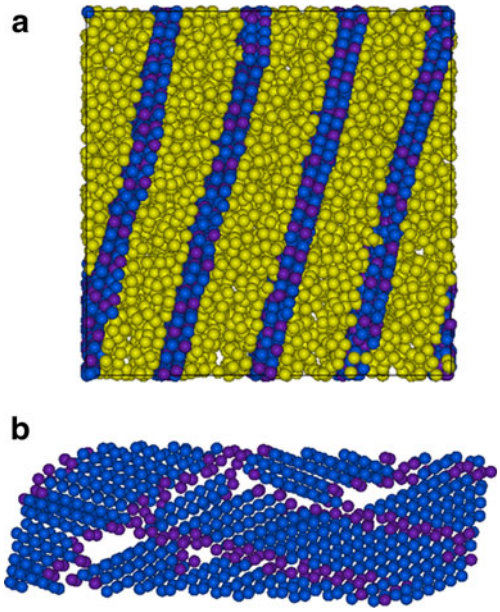

Fig. 5 **a** Bilayer sheets formed by TN3-258 at φ=0.3 and T*=1.3. Rod ends are colored *purple*. **b** A single bilayer sheet extracted from the simulation box; the tethers have been removed for clarity

of laterally tethered nanorods with three three-bead tethers. Total MSD and the two components, one along the normal of the bilayer sheet and the other in the bilayer sheet, are calculated. Tethered nanorods have greater mobility in the direction parallel to the layers for different number densities (Fig. S4).

End-tethered nanorods

The end-tethered nanorods we studied here are rods with a single nine-bead tether (TN1-1) or three three-bead tethers (TN3-1) grafted onto the end bead of the nanorod. The elastic stretching energy of the tethers becomes dominant and self-assembly structures with curve interfaces are preferred. The phase diagrams for these two models are presented in Fig. 7, which shows that the micelle structure and the cylinder structure are favorable. These structures are discussed in detail below.

Self-assembly of end-tethered nanorod with a nine-bead tether

TN1-1 For number densities between φ=0.1 and φ=0.4, the formation of micelle phase is observed at lower temperatures. Figure 8a presents a typical snapshot for a system at φ=0.3 and T^*=2.7. An individual micelle is extracted from the simulation box to illustrate the packing of the rods, as shown in Fig. 8b. The snapshot reveals that the rods pack with a twist and the tethers extend radially from the center of the micelle (Fig. 8c). To describe the shape of the micelles, we calculate the asphericity parameter defined in reference [8]

$$As = \frac{\sum_{i>j}^{3} \left\langle \left(R_i^2 - R_j^2 \right)^2 \right\rangle}{2 \left\langle \left(\sum_{i=1}^{3} R_i^2 \right)^2 \right\rangle} \tag{7}$$

where $R_i^2$is the eigenvalue of the gyration tensor of each micelle and<…>means that the average is performed over all micelles in the same size range. For a spherical micelle, the asphericity parameter is close to zero, whereas for a rod-like micelle, the asphericity parameter takes a value close to one. The asphericity parameter is plotted as a function of the micelle size and is shown in Fig. 9. The micelle size is defined as the number of tethered nanorods within a micelle. Figure 9 also shows the probability distribution of the micelle size, where small short-lived aggregates

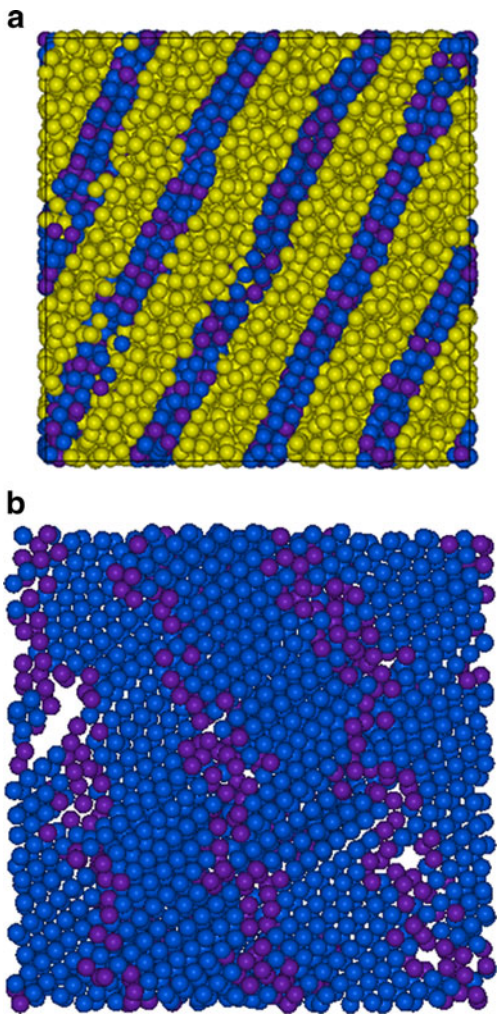

Fig. 6 **a** Bilayer sheets formed by TN3-258 at φ=0.6 and T*=2.0. Rod ends are colored *purple*. **b** A single bilayer sheet extracted from the simulation box; the tethers have been removed for clarity

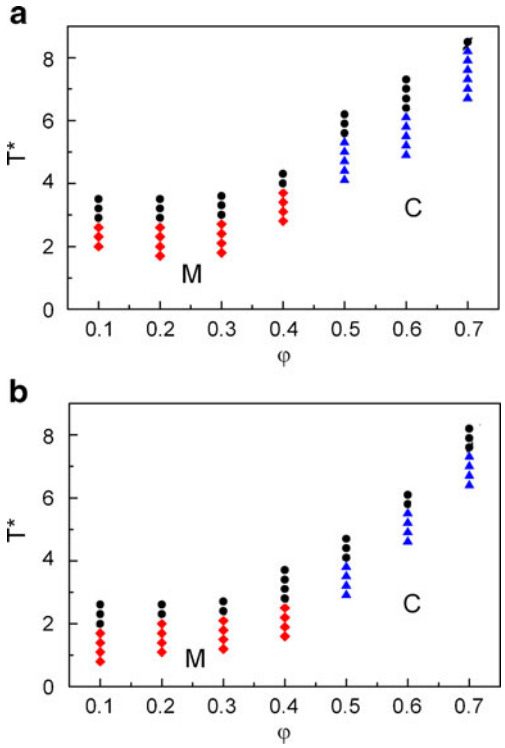

Fig. 7 Temperature vs number density phase diagrams for (**a**) TN1-1 and (**b**) TN3-1, respectively. *Red diamonds* Spherical micelle phase (*M*), *blue triangles* cylinder phase (*C*), *solid circles* disordered states

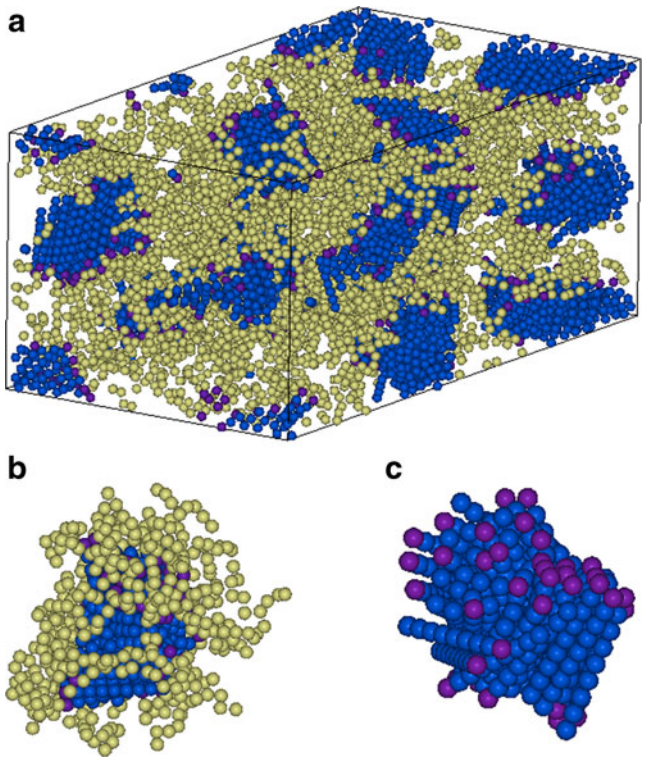

Fig. 8 **a** Spherical micelles formed by TN1-1 at φ=0.3 and T*=2.7. Rod ends with tethers are colored *purple*. **b** A single micelle, extracted from the simulation, consists of 54 tethered nanorods. **c** The core of the micelle in **b**; the tethers have been removed for clarity

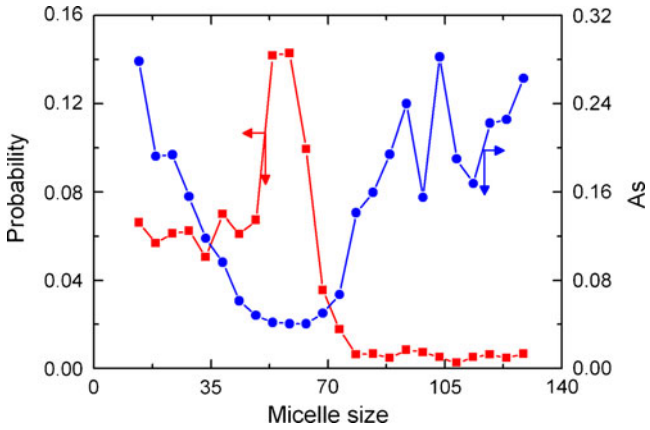

Fig. 9 Probability (left Y-axis) and asphericity parameter (right Y-axis) for TN1-1 at φ=0.3 and T*=2.7 as a function of micelle size. *Red squares* Probability, *blue circles* asphericity parameter

within which the number of tethered nanorods is less than 11 are ignored. Figure 9 reveals clearly that most of the micelles consist of 50–65 nanorods and the corresponding asphericity parameter is close to zero, indicating a preferred spherical micelle shape.

When the number density increases further, $\varphi > 0.4$, only the cylinder structure is stable. In contrast to the results obtained for end-tethered nanorods with lower aspect ratio [7–9], we did not observe long micelle phase in this research. Figure 10 shows a typical snapshot for a system at $\varphi = 0.5$ and $T^* = 4.5$. It reveals that the cylinders are nematically aligned and, within the cylinders, the rods pack with a twist about the cylinder axis. Compared with the

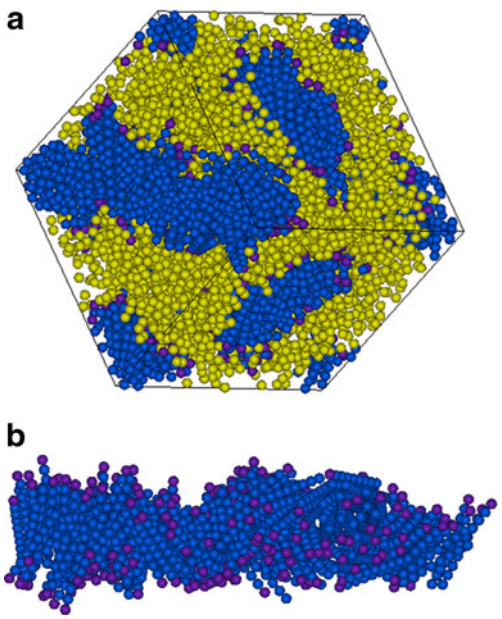

Fig. 10 **a** Cylinders formed by TN1-1 at φ=0.5 and T*=4.5. Rod ends with tethers are colored *purple*. **b** A single cylinder extracted from the simulation box; the tethers have been removed for clarity

chirally aligned cylinders formed by end-tethered nanorods with moderate aspect ratio, the cylinders obtained here do not exhibit chirality clearly, which may be a result of competition between the attractive interactions of the rods and the elastic interactions of the tethers. At constant tether fractions, rods with high aspect ratio have to twist quickly to lower the local grafting density of the tethers and hence compensate the increased elastic interactions between tethers. Additionally, the cylinder phase persists to higher number densities instead of the lamellar phase typically formed by end-tethered nanorods with lower aspect ratio at high densities [7–9]. It may also arise from the dominant elastic interactions between tethers with high local tether density in the case of nanorods with high aspect ratio, which strongly hinder the formation of lamellar structures in this study.

To illustrate the mobility of the end-tethered nanorods, MSD and the two components—one along the direction of the rod and the other vertical to the direction of the rod—are calculated. The results (Fig. S5) suggest that the mobility of the tethered rods is not strongly limited in the direction vertical to the rods, both for rods in micelle phase at low number densities and rods in cylinder phase at high number densities.

Self-assembly of end-tethered nanorod with three three-bead tethers

TN3-1 Similar to the phase behavior of TN1-1, the formations of the micelle phase at $\varphi<0.4$ and lower temperatures, and the nematic cylinder phase for $\varphi>0.4$ and relatively higher temperatures are observed for TN3-1, respectively. To determine the shape of the micelle phase at $\varphi=0.3$ and $T^*=1.7$ (Fig. S6), asphericity parameter is again employed. Plots of the asphericity parameter, as well as the probability distribution of different size micelles (Fig. S7) reveal that most micelles consist of 20–40 tethered nanorods and the corresponding asphericity parameter is less than 0.1, indicating that the micelles are basically spherical in shape. However, the rods in the micelles do not pack with a twist as in the case of TN1-1; they can be described more accurately as packing into an interdigitated structure, which is the result of the increased local grafting density. As the number density is increased further to $\varphi>0.4$, the nematic cylinder phase is observed. Compared with the cylinder formed by TN1-1, the rods here (Fig. S8) twist about the cylinder axis more quickly due to the increased local grafting density.

The mobility of TN3-1 is also described by MSD. MSD is resolved into two components: one along the direction of the rod and the other vertical to the direction of the rod. Like the results of TN1-1, the mobility of the TN3-1 rods is not strongly limited in the direction vertical to the rods, both for rods in micelle phase at low number densities and rods in cylinder phase at high number densities.

Conclusions

This paper presents the results of a study into the phase behavior of polymer-tethered nanorods with relative high aspect ratio of 9:1. We have demonstrated that the aspect ratio of the nanorods, and the number and the location of polymer tethers significantly affect both the mesophase behavior and local packing of self-assembled structures. For laterally tethered nanorods, rod–rod interactions are dominant and self-assembly structures with flat interfaces are preferred. Therefore, stepped ribbon phase and lamellar phase are observed. It is worth noting that the stepped lamellar phase is found for the first time in this research. When rods grafted with three tethers are distributed uniformly, lamellar phase with rods packed into bilayer sheets exists for the whole range of number densities in our study. For end-tethered nanorods, tether–tether interactions are dominant and the tethered nanorods self-assemble into structures with curved interfaces. Therefore, spherical micelle phase and nematic cylinder phase are formed. Instead of the lamellar phase typically found for nanorods with lower aspect ratio, the cylinder phase observed in this research persists to high number densities.

Acknowledgments This work is supported by National Natural Science Foundation of China (20974040, 50930001, 20933001), the Program for New Century Excellent Talents in University of China, Fok Ying Tung Education Foundation (114018).

References

1. Hermanson KD, Lumsdon SO, Williams JP, Kaler EW, Velev OD (2001) Dielectrophoretic assembly of electrically functional microwires from nanoparticle suspensions. Science 2:1082–1086
2. Crossland EJW, Kamperman M, Nedelcu M, Ducati C, Wiesner U, Smilgies DM, Toombes GES, Hillmyer MA, Ludwigs S, Steiner U, Snaith HJ (2009) A bicontinuous double gyroid hybrid solar cell. Nano Lett 9:2807–2812
3. Zhang XP, Sun BQ, Friend RH, Guo HC, Nau D, Giessen H (2006) Metallic photonic crystals based on solution-processible gold nanoparticles. Nano Lett 6:651–655
4. Shevchenko EV, Ringler M, Schwemer A, Talapin DV, Klar TA, Rogach AL, Feldmann J, Alivisatos AP (2008) Self-assembled binary superlattices of CdSe and au nanocrystals and their fluorescence properties. J Am Chem Soc 130:3274–3475
5. Zhang ZL, Horsch MA, Lamm MH, Glotzer SC (2003) Tethered nano building blocks: towards a conceptual framework for nanoparticle self-assembly. Nano Lett 3:1341–1346
6. Iacovella CR, Horsch MA, Glotzer SC (2008) Local ordering of polymer-tethered nanospheres and nanorods. J Chem Phys 129:044902
7. Horsch MA, Zhang ZL, Glotzer SC (2005) Self-assembly of polymer-tethered nanorods. Phys Rev Lett 95:056105

8. Horsch MA, Zhang ZL, Glotzer SC (2006) Simulation studies of self-assembly of end-tethered nanorods in solution and role of rod aspect ratio and tether length. J Chem Phys 125:184903
9. Horsch MA, Zhang ZL, Glotzer SC (2010) Self-assembly of end-tethered nanorods in a neat system and role of block fractions and aspect ratio. Soft Matter 6:945–954
10. Horsch MA, Zhang ZL, Glotzer SC (2006) Self-assembly of laterally-tethered nanorods. Nano Lett 6:2406–2413
11. Crane AJ, Martinez-Veracoechea FJ, Escobedo FA, Müller EA (2008) Molecular dynamics simulation of the mesophase behaviour of a model bolaamphiphilic liquid crystal with a lateral flexible chain. Soft Matter 4:1820–1829
12. Bates M, Walker M (2009) Dissipative particle dynamics simulation of T- and X-shaped polyphilic molecules exhibiting honeycomb columnar phases. Soft Matter 5:346–353
13. Zehla T, Wahaba M, Schmidta R, Schillera P, Mögel HJ (2009) Monte Carlo studies on self-assembly of surfactants in aqueous solutions. J Mol Liq 147:178–181
14. Wahab M, Schiller P, Schmidt R, Mögel HJ (2010) Monte Carlo study of the self-assembly of achiral bolaform amphiphiles into helical nanofibers. Langmuir 26:2979–2982
15. Pryamitsyn V, Ganesan V (2004) Translocation of a b-hairpin-forming peptide through a cylindrical tunnel. J Chem Phys 120:5824
16. Chen JZ, Zhang CX, Sun ZY, Zheng YS, An LJ (2006) A novel self-consistent-field lattice model for block copolymers. J Chem Phys 124:104907
17. Reenders M, ten Brinke G (2002) Compositional and orientational ordering in rod-coil diblock copolymer melts. Macromolecules 35:3266–3280
18. He L, Zhang L, Ye Y, Liang H (2010) Solvent-induced self-assembly of polymer-tethered nanorods. J Phys Chem B 114:7189–7200
19. Iacovella CR, Glotzer SC (2009) Complex crystal structures formed by the self-assembly of ditethered nanosphere. Nano Lett 9:1206–1211
20. Iacovella CR, Glotzer SC (2009) Phase behavior of ditethered nanospheres. Soft Matter 5:4492–4498
21. Chan ER, Zhang X, Lee CY, Neurock M, Glotzer SC (2005) Simulations of tetra-tethered organic/inorganic nanocube-polymer assemblies. Macromolecules 38:6168–6180
22. Zhang X, Zhang ZL, Glotzer SC (2007) Simulation study of cyclic-tethered nanocube self-assemblies: effect of tethered nanocube architectures. Nanotechnology 18:115706. doi:10.1088/0957-4484/18/11/115706
23. Lamm MH, Chen T, Glotzer SC (2003) Simulated assembly of nanostructured organic/inorganic networks. Nano Lett 3:989–994
24. Zhang X, Chan ER, Glotzer SC (2005) Self-assembled morphologies of monotethered polyhedral oligomeric silsesquioxane nanocubes from computer simulation. J Chem Phys 123:184718
25. Nguyen TD, Zhang Z, Glotzer SC (2008) Molecular simulation study of self-assembly of tethered V-shaped nanoparticle. J Chem Phys 129:244903
26. Elmahdy MM, Floudas G, Mondeshki M, Spiess HW, Dou X, Müllen K (2008) Origin of the complex molecular dynamics in functionalized discotic liquid crystals. Phys Rev Lett 14:107801
27. Andrienko D, Marcon V, Kremer K (2006) Analytical linearized Poisson–Boltzmann approach: beyond the generalized born approximation. J Chem Phys 125:124902
28. Yan F, Hixson CA, Earl DJ (2008) Self-assembled chiral superstructures composed of rigid achiral molecules and molecular scale chiral induction by dopants. Phys Rev Lett 101:157801
29. Yan F, Hixson CA, Earl DJ (2009) Computer simulations of linear rigid particles that form chiral superstructures and tilted smectic phases. Soft Matter 5:4477–4483
30. Smith W, Forester TR (1996) DL_POLY_2.0: a general-purpose parallel molecular dynamics simulation package. J Mol Graph 14:136–141
31. Miller T, Eleftheriou M, Pattnaik P, Ndirango A, Newns D, Martyna G (2002) Symplectic quaternion scheme for biophysical molecular dynamics. J Chem Phys 116:8649